Marine Pollution Bulletin
March 2023, Volume 188 Pages 114629 (9p.)
https://doi.org/10.1016/j.marpolbul.2023.114629
https://archimer.ifremer.fr/doc/00822/93349/

A new Sargassum drift model derived from features tracking in MODIS images

Podlejski Witold [1, 2, *], Berline Léo [1], Nerini David [1], Doglioli Andrea [1], Lett Christophe [2]

[1] Aix Marseille Univ, Université de Toulon, CNRS, IRD, MIO, Marseille, France
[2] Marbec, Université de Monpellier, CNRS, Ifremer, IRD, Sète, France

* Corresponding author : Witold Podlejski, email address : witold.podlejski@mio.osupytheas.fr

Abstract :

Massive Sargassum stranding events affect erratically numerous countries from the Gulf of Guinea to the Gulf of Mexico. Forecasting transport and stranding of Sargassum aggregates require progress in detection and drift modelling. Here we evaluate the role of currents and wind, i.e. windage, on Sargassum drift. Sargassum drift is computed from automatic tracking using MODIS 1 km Sargassum detection dataset, and compared to reference surface current and wind estimates from collocated drifters and altimetric products. First, we confirm the strong total wind effect of ≈3 % (≈2 % of pure windage), but also show the existence of a deflection angle of ≈10° between Sargassum drift and wind directions. Second, our results suggest reducing the role of currents on drift to 80 % of its velocity, likely because of Sargassum resistance to flow. These results should significantly improve our understanding of the drivers of Sargassum dynamics and the forecast of stranding events.

Highlights

► Automatic tracking of *Sargassum* aggregations on MODIS coarse resolution ► 200-cases dataset of *Sargassum* velocities ► Wind effect evaluated at 3 % of the wind speed, deviated 10° to the right. ► Currents effect evaluated at 80 % its full speed.

Keywords : Sargassum algae, Computer vision, Regression, Tracking, Remote sensing, Drift, Collocation, Drifter, Tropical North Atlantic, Time series

1. Introduction

In recent years, the extent of the Great Atlantic *Sargassum* Belt (GASB) has stabilized to a high level of *Sargassum* biomass associated with harmful stranding events. Countries affected by stranding along their coast are struggling to face the economical, ecological and sanitary damages (Van Tussenbroek et al., 2017; Resiere et al., 2018; Rodríguez-Martínez et al., 2019; Chávez et al., 2020; Merle et al., 2021; de Lanay et al., 2022). As a consequence, strong efforts are put in monitoring *Sargassum* distribution (Gower & King, 2011; Wang & Hu, 2016; Cuevas et al., 2018; Wang et al., 2019; Ody et al., 2019; Descloitres et al., 2021) and modelling *Sargassum* drift and growth (Putman et al., 2018; Brooks et al., 2018; Beron-Vera & Miron, 2020; Jouanno et al., 2021b).

As for several other surface drifting objects, most models of *Sargassum* drift included a windage component (Kwon et al., 2019; Putman et al., 2020; Berline et al., 2020; Johns et al., 2020; Jouanno et al., 2021a) to represent the direct effect of wind and waves on drift velocity. Model results were shown to be sensitive to windage (Kwon et al., 2019; Putman et al., 2020; Berline et al., 2020; Miron et al., 2020) and it is therefore

key to estimate this factor accurately. Up to now, windage was tested in simulations and calibrated with either *in-situ* or remote sensing data (Kwon et al., 2019; Putman et al., 2020; Berline et al., 2020; Jouanno et al., 2021a). However, except for Putman et al. (2020) who used a limited number of *Sargassum* rafts tracked trajectories, there is currently no direct measure of windage.

Satellite imagery may allow tracking *Sargassum* aggregates displacement on images in order to extract velocity and estimate windage. However, *Sargassum* detection from space is hampered by the high cloud coverage and aggregates shapes change rapidly, therefore a short satellite revisit time is necessary in order to track aggregates. High resolution sensors (e.g., MSI, Landsat8) allow describing the fine scale structure of aggregates (Ody et al., 2019; Descloitres et al., 2021) but their revisit time (5-8 days) precludes aggregate tracking from one image to the next. Moderate-Resolution Imaging Spectroradiometer (MODIS), with two daily observations separated by approximately 3 hours, is best suited for tracking *Sargassum* aggregates.

Here, we used successive MODIS *Sargassum* detection images provided by Podlejski et al. (2022) over the 2015-2021 period and applied computer vision tracking algorithms to compute *Sargassum* velocity. We then used complex linear regressions to relate this velocity to estimates of currents and wind derived from altimetry and velocity of collocated drifters (Lumpkin & Pazos, 2007) and to assess windage. Finally, we propose a new model of *Sargassum* drift.

2. Materials and Methods

2.1. Overview

An overview of the whole approach made to extract *Sargassum* drift is shown in Fig. 1. First, *Sargassum* detections mapped at 1 km resolution from MODIS Aqua and Terra were collected from `https://doi.org/10.12770/8fe1cdcb-f4ea-4c81-8543-50f0b39b4eca`. The production process is described in Descloitres et al. (2021) for extracting the Alternative Floating Algae Index (AFAI) and deducing *Sargassum* coverage. The filtering method developed in Podlejski et al. (2022) was used to remove the false detections (false positive) caused by cloud, sunglint or coastal contamination. We used here filtered daily images at 1 km resolution. Among these images, we selected daily scenes with both Aqua and Terra clear *Sargassum* observations. For the comparison between *Sargassum* and drifters velocities, the Global Drifter Program (GDP) (Lumpkin & Pazos, 2007) data were collected and collocation cases (simultaneous presence in a range of 20 km) between *Sargassum* and drifters were extracted (Appendix A). The dataset of collocation was split between drogued drifters and undrogued drifters.

MODIS images were analysed with computer vision algorithms to match *Sargassum* aggregates from successive images and thereby derive their velocity (section 2.2). This matching process was validated manually to ensure reliability of measurements. Then, geostrophic currents and wind were interpolated at the position and time of each measurement (section 2.3). Finally, a statistical analysis was performed in order to infer the links between the velocities of *Sargassum* aggregates, drifters, surface current and wind, using linear regressions in the complex space (section 2.4).

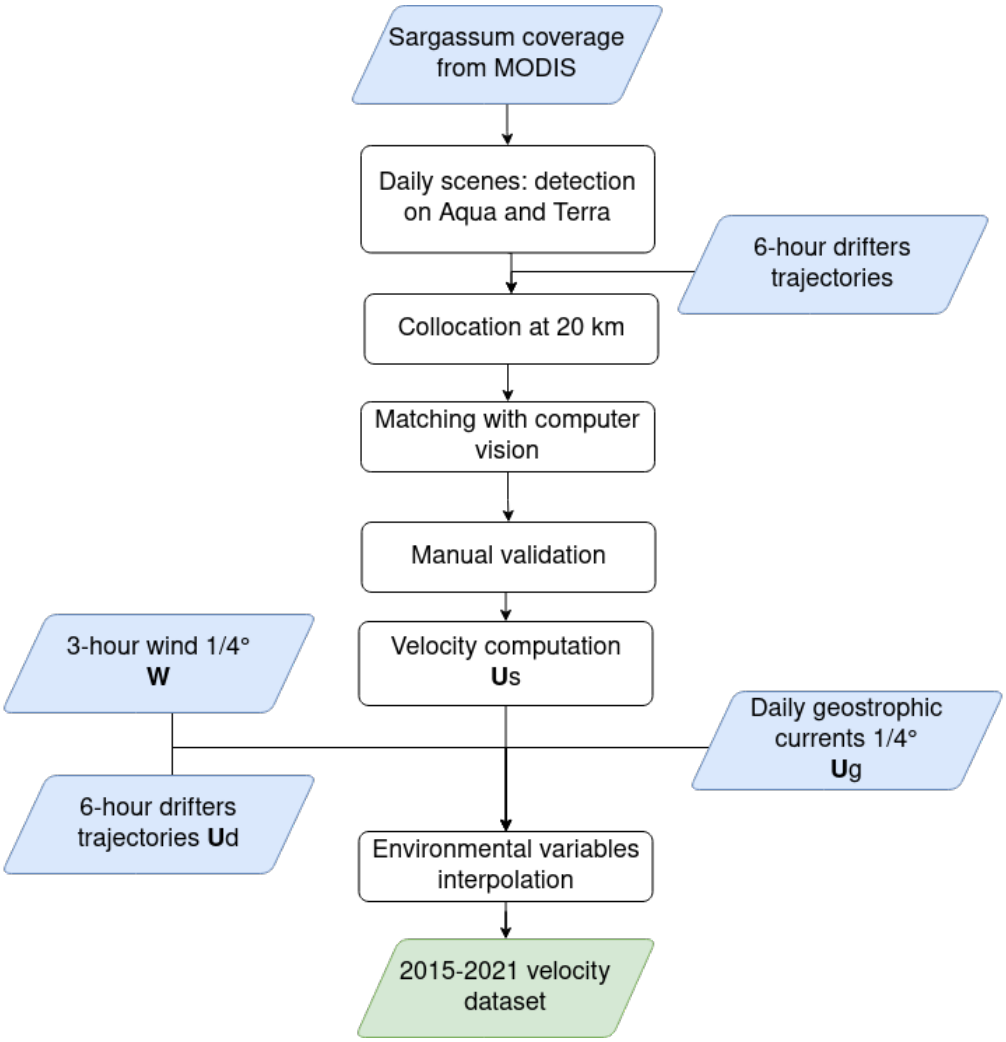

Figure 1: Workflow of the *Sargassum* aggregates velocity extraction process, with data sources indicated in blue, results in green and processes in white. $\mathbf{W}$, $\mathbf{U}_d$, $\mathbf{U}_S$, $\mathbf{U}_G$ are wind, drifter, *Sargassum* and geostrophic current velocities, respectively.

2.2. Images matching to derive Sargassum velocity

Based on the two daily MODIS images of selected *Sargassum* aggregates, a matching process was performed in order to retrieve the two successive positions of the aggregate and thereby estimate its velocity. Two different algorithms were applied on a 100 * 100 km AFAI images subset around the collocated drifter position (50 km range), namely Scale Invariant Feature Transform (SIFT) (Lowe, 2004) and optical flow (OF) as implemented in Farnebäck (2003). Lucas-Kanade (Lucas et al., 1981) and Gradient Location and Orientation Histogram (GLOH) (Mikolajczyk & Schmid, 2005) algorithms were tested on the images, but showed lower performances. All image processing was performed with Python 3 and the OpenCV library.

SIFT was used to extract key points for describing aggregates shape based on Terra and Aqua AFAI images. Using these key points, the best subset of congruent linear 2D translations (no scaling, no rotation)

was extracted, and averaged to compute the corresponding *Sargassum* velocity (see Appendix B). Then, OF algorithm was applied to confirm SIFT results. Inconsistent cases between the drift directions estimated from SIFT and OF were rejected, i.e., when the absolute angle between the estimated directions was larger than 25°. We retained velocity from SIFT as it was found more robust than OF.

Finally, a manual validation was performed on all remaining cases, based on an overall visual inspection of matching cases with a focus on all matching pairs of key points to ensure they were valid.

2.3. Current and wind velocities

As a direct estimation of the surface current, we used drifter data. The drifter data were downloaded from the GDP website (`https://www.aoml.noaa.gov/phod/gdp/`, Lumpkin & Centurioni (2019)). The Surface Velocity Program (SVP) drifters are made of a low-windage surface satellite transmitter (35 cm spherical hull) tethered by a thin cable to a semi-rigid sea anchor (the so-called "Holey-Sock" drogue) centred at 15 m depth. These properties allow drifters to follow reliably the 15 m depth currents. When a drifter loses its drogue, it tends to follow the surface current, but with a non-negligible effect of wind.

As an indirect estimation of the ocean surface current, we used the altimetry-derived geostrophic velocity at 1/4 °daily resolution available from `www.aviso.altimetry.fr`. Altimetry-derived current was considered as the local surface current not affected by wind.

As estimation of the surface wind velocity, we used the 10-metre wind from ECMWF ERA5 reanalysis at the 1/4 °hourly resolution (Hersbach & Dee, 2016) (from https://cds.climate.copernicus.eu/)

After extraction, both surface current and wind fields were interpolated at the position and time of each collocated *Sargassum* aggregate/drifter pair.

2.4. Statistical analyses

The overall idea here is to analyse to what extent the surface current, either from geostrophic estimates or from collocated drifters, and the wind can explain the *Sargassum* aggregate velocity measured from MODIS images.

We used the complex notation for vectors (Kundu, 1976; Poulain et al., 2009; Sutherland et al., 2020):

$$\mathbf{U} = re^{i\theta} \; or \; u + iv \tag{1}$$

with $\mathbf{U}$ a velocity vector expressed as a complex number, r its norm, θ its argument (between $-\pi$ and π, anticlockwise) and u, v the eastward and northward components of the velocity.

A general model of *Sargassum* velocity $\mathbf{U}_S$ can be written as follows (Mulet et al., 2021):

$$\mathbf{U}_S = \mathbf{U}_G + \mathbf{U}_A + \varepsilon = \mathbf{U}_G + \mathbf{U}_T + \mathbf{U}_I + \mathbf{U}_E + \mathbf{U}_{St} + \mathbf{U}_W + \varepsilon \tag{2}$$

where $\mathbf{U}_G$, $\mathbf{U}_A$, $\mathbf{U}_T$, $\mathbf{U}_I$, $\mathbf{U}_E$, $\mathbf{U}_{St}$, $\mathbf{U}_W$ and ε are the *Sargassum*, the geostrophic current, the ageostrophic current, the tidal current, the inertial current, the Ekman current, the Stokes drift, the windage and the error

term, respectively. The tidal current is considered negligible in the offshore cases studied. At the latitudes of interest (0 to 25°N) the Coriolis force is weak. Inspection of drifters trajectories near the collocations revealed only a few (<10) cases of inertial oscillations. As a consequence, we consider the inertial current as negligible. Following Van Sebille et al. (2020), we assume that the Stokes drift and the windage can be combined. The Ekman current is also due to the wind forcing, these three terms can therefore be combined in a unique term depending on the wind:

$$\mathbf{U}_S = \alpha_G^S \mathbf{U}_G + \beta_G^S \mathbf{W} + \varepsilon \tag{3}$$

where $\mathbf{W}$ is the wind and α_G^S and β_G^S are complex parameters. The parameter α_G^S represents the role of geostrophic current on *Sargassum* aggregate drift, and the parameter β_G^S represents the effect of Ekman current, Stokes drift and windage. Similarly, drifter velocity can be expressed as follows:

$$\mathbf{U}_D = \alpha_G^D \mathbf{U}_G + \beta_G^D \mathbf{W} + \varepsilon \tag{4}$$

with $\mathbf{U}_D$ the drifter velocity. Here the β_G^D parameter depends largely on whether the drifter has lost its drogue or not. We thus estimated this parameter separately for drogued and undrogued drifters.

We can also relate directly *Sargassum* and drifters velocities using the following models:

$$\mathbf{U}_S = \alpha_{D,d}^S \mathbf{U}_{D,d} + \beta_{D,d}^S \mathbf{W} + \varepsilon \tag{5}$$

$$\mathbf{U}_S = \alpha_{D,u}^S \mathbf{U}_{D,u} + \beta_{D,u}^S \mathbf{W} + \varepsilon \tag{6}$$

where $\mathbf{U}_{D,d}$, $\mathbf{U}_{D,u}$ are the velocities for drogued and undrogued drifters, respectively. Here the β_D^S parameter does not include the effect of $\mathbf{U}_E$ which is included in the α_D^S parameter.

For all models, we used linear regressions in the complex space to find the set of complex parameters minimising the error ε (Appendix C).

Also, the models were tested using Ekman-corrected velocities to distinguish between Ekman component and windage (Appendix E). Real parameters (no angle) used in the literature were tested for comparison. Each regression was evaluated with the coefficient of determination R^2 (square of the real part of the complex correlation coefficient). Significance tests were applied for both models (Fisher test) and parameters (Student test). The bootstrap method was set up to estimate robust parameters, their confidence interval and the associated coefficient of determination (see Appendix D).

In order to further refine the regression models, outliers were isolated. Based on leave one out, the distance (error) between observations and model predictions was computed. By looking at the largest computed distance values, 4 cases were excluded where the *Sargassum* velocity direction was opposite to both wind and geostrophic currents.

3. Results

Over the period 2015-2021, we found 2754 cases of a *Sargassum* aggregate detected in both MODIS Terra and Aqua images and with a drifter of the Global Drifter Program passing by (see Tab. 1). Among them, for 240 cases we managed to match the *Sargassum* aggregate in Terra and Aqua images and could therefore estimate the aggregate velocity. An illustrative example of the matching process using SIFT is shown in Fig. 2. Our manual validation filtered out 48 more cases, and we ended up with 192 cases, 98 with a collocated drogued drifter and 94 with an undrogued drifter. This strict selection guarantees the estimates' accuracy of the drift velocity and a sufficient dataset for further statistical analysis.

Year	2015	2016	2017	2018	2019	2020	2021	All
Daily scenes	341	98	204	713	461	515	422	2754
Matching collocations	23	2	19	65	51	47	33	240
Valid drogued collocations	13	1	10	24	17	27	11	98
Valid undrogued collocations	3	1	9	26	26	14	16	94

Table 1: Number of collocation cases per year at different steps of the method. First after selection of the daily scenes with detections on Terra and Aqua, second after performing matching algorithms and finally after manual validation.

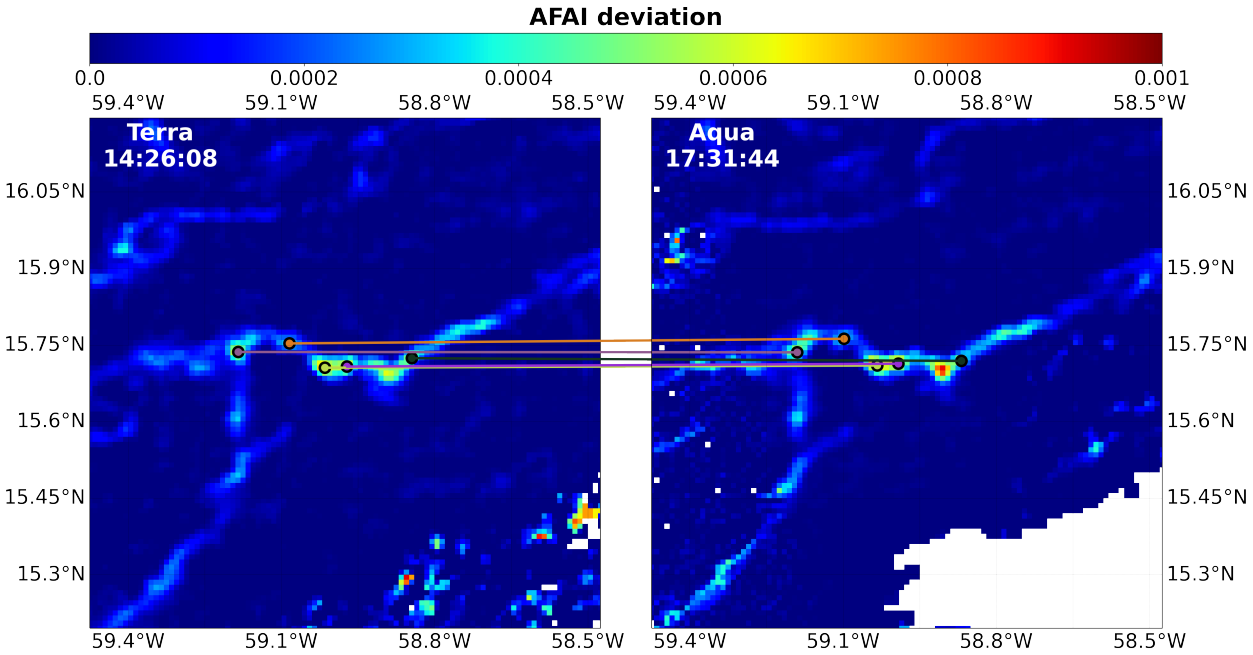

Figure 2: Example of image matching of January 6th 2021 for a collocated case with SIFT key points extracted from Terra and Aqua 100 x 100 pixels images. The five consistent matches are shown as linked pairs of points. The colorbar refers to AFAI deviation from background (Podlejski et al., 2022), the white area is the mask. The collocated drifter is located at the centre of each image (not shown).

The distribution of these cases with respect to time and space is shown in Fig. 3. Fig. 4 shows the distribution of the intensity and direction of velocities for the detected *Sargassum* aggregates, collocated drifters, and interpolated geostrophic current and wind at the time and position of the collocated drifters.

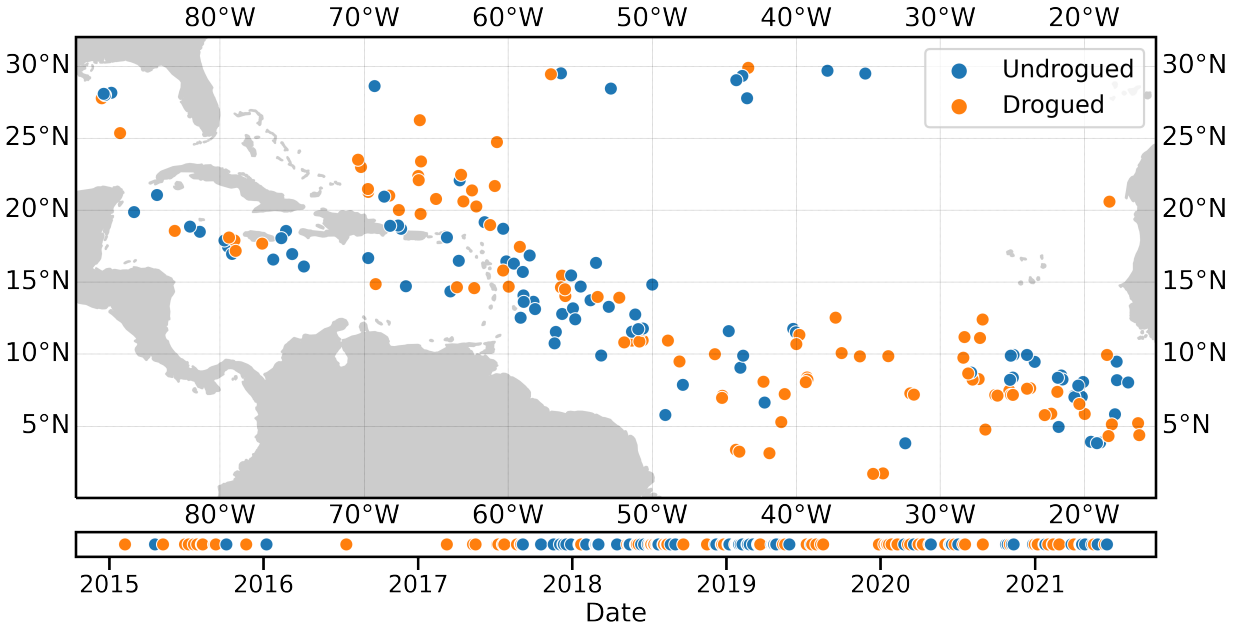

Figure 3: Collocated *Sargassum*/drifter pairs (n = 192) distribution in space and time, split into drogued (orange) and undrogued (blue) drifters.

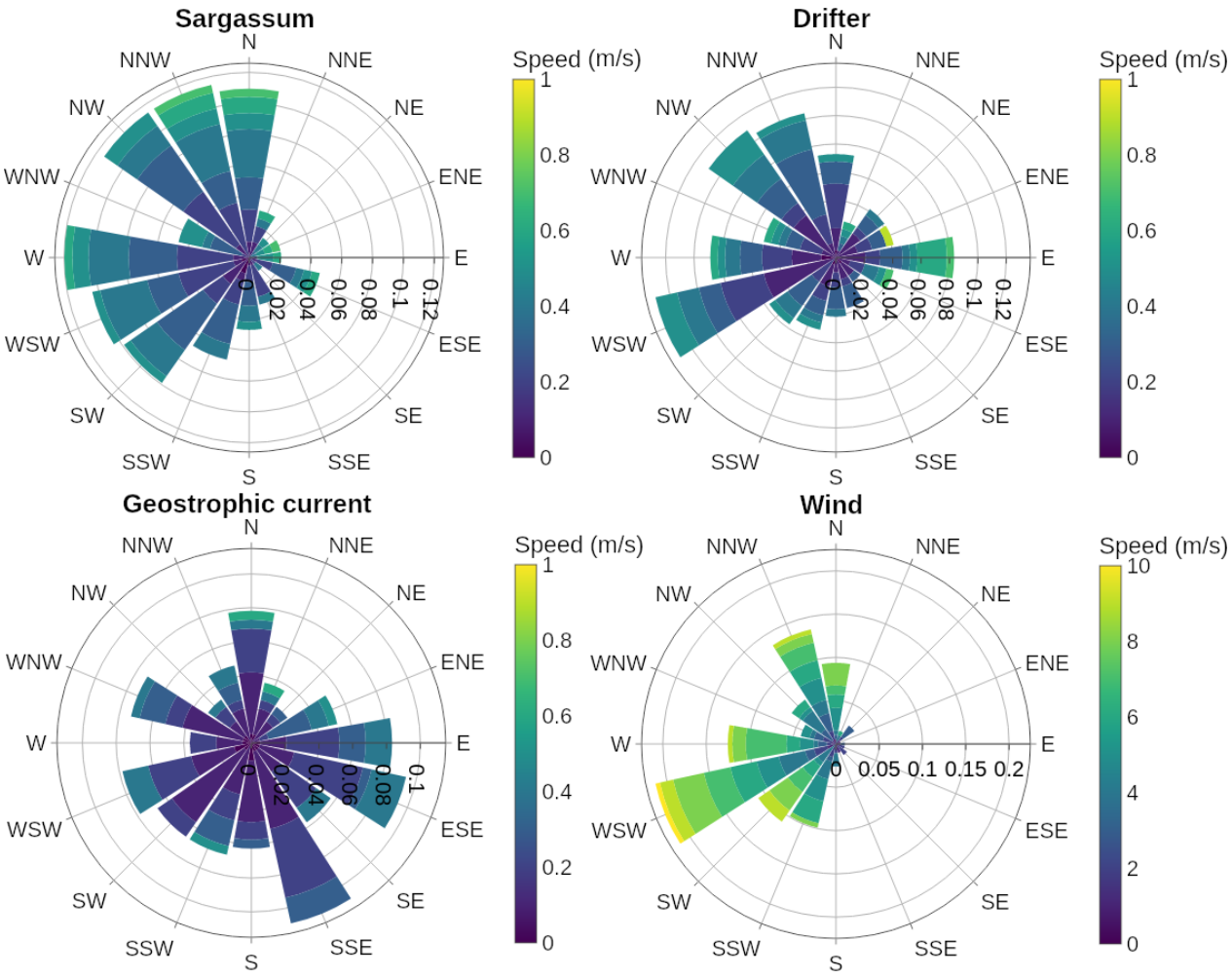

Figure 4: Wind-rose of velocities for the detected *Sargassum* aggregates, collocated drifters (drogued and undrogued), and interpolated geostrophic current and wind at the time and location of the collocated drifters. Colours indicate the speed, and bar lengths the frequency. Note that all velocity directions are expressed in terms of vector azimuth, i.e. the direction toward which the vectors lead.

Collocated *Sargassum*/drifter pairs were homogeneously distributed in the area of *Sargassum* presence along the time series 2015-2021 (Fig. 3). Geostrophic currents had a rather uniform orientation distribution, whereas *Sargassum*, drifter and wind velocity orientations were primarily westward (Fig. 4). The 4 variables are correlated. The correlation coefficients (norm of the complex coefficients) for $\mathbf{U}_S$ against $\mathbf{U}_D$ and $\mathbf{U}_G$ are 0.80 and 0.47, respectively. While $\mathbf{W}$ against $\mathbf{U}_D$ correlation was 0.37 and $\mathbf{W}$ against $\mathbf{U}_G$ correlation was only 0.18.

In a first set of regression models, we explored the relation of *Sargassum* velocity $\mathbf{U}_S$ and drifter velocity $\mathbf{U}_D$ against geostrophic and wind velocities $\mathbf{U}_G$ and $\mathbf{W}$ (Tab. 2). We obtained statistically significant correlations in all tested models, but with weak coefficients of determination R^2(maximum of 0.47). All parameters bootstrapped means were consistent with the direct parameter estimation (not shown) and their

standard deviation was approximately 10% of their value. Geostrophic current $\mathbf{U}_G$ was projected on $\mathbf{U}_S$ and $\mathbf{U}_D$ with small angle values (-14°to 7°). The norm of the geostrophic current coefficient was always smaller than 1 (0.59 to 0.85). Wind velocity was projected with an angle of 15-65 °to the right of the wind direction, the angle estimation was weakly variable (±5°). The norm of the wind coefficient corresponded to 3-4% of its velocity for *Sargassum* and undrogued drifters, whereas drogued drifters were impacted by 1% of the wind velocity only.

Model	α	β	R^2	N_{obs}
$\mathbf{U}_S = \alpha_G^S \mathbf{U}_G + \beta_G^S \mathbf{W}$	$0.593 \pm 0.065 \exp(-14.0 \pm 8.8°i)$	0	-0.02	192
	0	$0.038 \pm 0.003 \exp(-17.4 \pm 3.5°i)$	0.26	192
	$0.564 \pm 0.055 \exp(1.6 \pm 5.4°i)$	$0.038 \pm 0.002 \exp(-21.2 \pm 3.0°i)$	0.46	192
$\mathbf{U}_{D,u} = \alpha_G^{D,u} \mathbf{U}_G + \beta_G^{D,u} \mathbf{W}$	$0.778 \pm 0.083 \exp(-11.5 \pm 8.5°i)$	0	0.10	94
	0	$0.033 \pm 0.004 \exp(-14.9 \pm 5.9°i)$	0.18	94
	$0.659 \pm 0.077 \exp(0.6 \pm 7.1°i)$	$0.031 \pm 0.003 \exp(-21.4 \pm 5.8°i)$	0.43	94
$\mathbf{U}_{D,d} = \alpha_G^{D,d} \mathbf{U}_G + \beta_G^{D,d} \mathbf{W}$	$0.8 \pm 0.073 \exp(6.3 \pm 5.2°i)$	0	0.38	98
	0	$0.01 \pm 0.003 \exp(-64.2 \pm 35.1°i)$	0.02	98
	$0.852 \pm 0.068 \exp(6.7 \pm 4.4°i)$	$0.013 \pm 0.003 \exp(-61.4 \pm 13.7°i)$	0.47	98

Table 2: Regression models between measured velocities and environmental variables. $\mathbf{U}_S$, $\mathbf{U}_{D,d}$, $\mathbf{U}_{D,u}$, $\mathbf{U}_G$ and $\mathbf{W}$ are velocities for the detected *Sargassum* aggregates, collocated drogued/undrogued drifters, and interpolated geostrophic current and wind at the time and location of the *Sargassum* aggregates. Variables and estimated parameters are complex numbers, here displayed in exponential notation with angles in degrees anticlockwise. Depending on the regression model, some parameters are forced to real values (zero). The norm and the argument are associated with a standard deviation estimated over 5000 bootstrapped datasets. All regressions were statistically significant ($p < 0.01$), negative R^2 is due to model constraint (no intercept).

In a second set of regression models, we explored the relation of $\mathbf{U}_S$ against $\mathbf{U}_D$ and $\mathbf{W}$. (Tab. 3). We found much higher R^2 values (0.55-0.78) than for the first set of regressions. R^2 values were smaller for undrogued than for drogued drifters, and associated parameters were also generally more variable. The wind coefficient given by the regressions was 2-3%, deviated to the right of the wind.

Model	α	β	R^2	N_{obs}
$\mathbf{U}_S = \alpha_{D,u}^S \mathbf{U}_{D,u} + \beta_{D,u}^S \mathbf{W}$	$0.957 \pm 0.042 \exp(0.6 \pm 2.7°i)$	0	0.62	94
	$0.681 \pm 0.048 \exp(4.3 \pm 4.1°i)$	$0.021 \pm 0.003 \exp(-23.1 \pm 7.6°i)$	0.66	94
	1	0.01	0.57	94
$\mathbf{U}_S = \alpha_{D,d}^S \mathbf{U}_{D,d} + \beta_{D,d}^S \mathbf{W}$	$0.889 \pm 0.048 \exp(4.9 \pm 3.4°i)$	0	0.55	98
	$0.787 \pm 0.038 \exp(-2.3 \pm 2.9°i)$	$0.029 \pm 0.002 \exp(-8.6 \pm 4.2°i)$	0.78	98
	1	0.03	0.74	98

Table 3: Regression models for *Sargassum* velocity using drifters velocity as explaining variable. Same as Tab. 2

4. Discussion

4.1. General drift patterns

We found drifter and *Sargassum* velocities directed mainly westward. Indeed, most *Sargassum* detections are located in the tropical Atlantic (0-20°N, Fig. 3). In this region, trade winds are westward, as are the main surface currents (North and South Equatorial Currents and their branches). The only eastward current is the North Equatorial Counter Current at 7°N (Johns et al., 2020). The drifter and *Sargassum* velocities range ($< 0.9\,\mathrm{m\,s^{-1}}$) is typical for offshore surface currents, with *Sargassum* median velocity slightly higher than drifters (0.31 vs $0.24\,\mathrm{m\,s^{-1}}$).

4.2. Extraction of Sargassum velocities: method limitations

In the absence of *in situ* validation data, we assessed the velocities $\mathbf{U}_S$ of *Sargassum* aggregates measured in MODIS successive images by comparing them with independent velocities $\mathbf{U}_D$ of collocated surface drifters and local geostrophic currents $\mathbf{U}_G$. The good correlation (0.8, p-value < 0.01) obtained for $\mathbf{U}_S$ against $\mathbf{U}_D$ gives us confidence in the reliability of our method for extracting *Sargassum* velocities. The average *Sargassum* drift distance between successive images was 3.4 km. As the image's resolution was mapped at 1 km, the measurements have inherent uncertainty (Masuoka et al., 1998), but the redundancy between matching pairs of pixels used in the images (from 4 up to 20) allowed us to stand out from noise and to ensure their robustness. Other methods to derive current velocity from satellite images (Maximum Cross Correlation, e.g. Barton (2002), Yang et al. (2015)) used all pixels in the image with similar temporal offset (1-4 hours) and resolution (1 km) as ours. In comparison, our sparse approach (few key points instead of all pixels) with SIFT allows focusing only on relevant descriptors of the *Sargassum* shape and to easily select the velocity summarising the overall transport.

The distance used to consider *Sargassum* and drifters as collocated was set to 20 km as a compromise to obtain a significant number of collocation cases and to support the assumption that environmental variables (wind and currents) are the same for both objects. For the image matching process, we used a 50 km range around the drifter in order to benefit from more key points and context. The two distance values are smaller than the Rossby radius of deformation, i.e., the scale of current autocovariance, estimated > 60 km at latitudes $< 20°$(Chelton et al., 1998).

Given these methodological choices and the 6 year-long time series of daily data, only a limited number (200) of *Sargassum* velocities were retrieved. This is mostly due to high cloud coverage ($> 60\%$ on average for daily images) in the tropical Atlantic area that prevented matching aggregates in successive images. Also, significant distortion of aggregates between images and their elongated shapes (e.g., linear aggregates provide few key points) prevented matching. Several solutions could be pursued to expand this dataset. Manual matching could be pursued to complement velocity extraction, but with presumably small amount of new scenes. The matching process could be extended to others collocated tracked objects, such as Fish Aggregating Devices (Imzilen et al., 2019). We could also try to match aggregates more distant in time.

However, the match would hardly be automatic, because of the distortion increasing over time, but could be performed manually for specific regions or time of interest. Using other satellite products, such as Visible Infrared Imaging Radiometer Suite (VIIRS) or Geostationary Operational Environmental Satellite (GOES) could also be a way to expand our dataset of *Sargassum* velocities. Indeed, preliminary results suggest that VIIRS gives results analogous to MODIS (Wang & Hu, 2020) and that GOES seems promising due to its high temporal resolution (Minghelli et al., 2021).

4.3. Physical and statistical approximations

The Stokes drift was considered combined to wind effect. Replacing **W** by Stokes velocity from ECMWF ERA5 decreased the R^2 values (not shown). Adding Stokes velocity as an additional explanatory variable in the regressions was associated with non-significant p-value and negligible R^2 improvement, as Stokes velocity was highly correlated with wind velocity (r=0.83). More accurate data are needed to separate the effect of Stokes drift and wind in the windage, similarly to Sutherland et al. (2020).

For all the models, we chose to force the regressions with no intercept (constant term) as it is hardly interpretable physically. When an intercept was included, regressions with two variables did not show major R^2 improvement nor changes of parameter values, because the intercept term was very low ($<0.05\,\mathrm{m\,s^{-1}}$). This validates our hypothesis of null intercept and indicates that the results were weakly biased, and the models were linear. As the distribution of residuals is Gaussian (not shown), the remaining unexplained variability is likely due to the uncertainty of observations. Improving the result probably lies in better data accuracy.

4.4. Geostrophic component of Sargassum drift

The comparison between drifter and *Sargassum* regression models provides good indications on how *Sargassum* drift differs from drifters. First, on average, the geostrophic current component is not deviated for *Sargassum* velocity (low α_G^S angle), and this is also true for drifters. This confirms our hypothesis of negligible inertial effect for these objects at the considered timescale (3 hours). This contrasts with Brooks et al. (2019)'s result, likely because of their much larger timescale (8 days).

Second, drifter velocity is explained by a fraction of geostrophic current velocity (α_G^D=85% for drogued drifters and 66% for undrogued drifters). This is also true when using Ekman-corrected drifter velocities (Appendix E). This contrasts with previous studies showing that the Ekman-corrected drifter velocities were on average 1.4 times higher than the altimeter-derived geostrophic currents (Lagerloef et al. (1999)). These contrasting results are likely due to major progress in spatial and temporal resolutions of both altimetric product (1/4°daily data used here vs. 1°10-day data in Lagerloef et al. (1999) and drifter position frequency (6-h here vs. 5-day in Lagerloef et al. (1999)). The parameter α_G^D was found < 1 possibly because of the fine scale variability of drifters velocities that are not captured by altimetry. In addition, as the α_G^S parameter was weaker than α_G^D ($< 56\%$), this suggests a flow resistance (i.e. viscosity) of *Sargassum* aggregates that slows them down compared to local currents and nearby drifters.

4.5. Windage and Ekman component of Sargassum drift

The parameter β_G^S, i.e. the wind effect on *Sargassum* drift, was deviated to the right of the wind direction with an angle of 21° while $\beta_{D,d}^S$ is deviated with an angle of 9° (Tab. 2 and 3). Deviation to the right of the wind is expected from Ekman spiral theory (Ekman, 1905). As $\mathbf{U}_S$ and $\mathbf{U}_D$ included the Ekman current, β_D^S is a combination of Ekman current (45° at the surface) and windage (weak deflection). This is confirmed by regressions performed on $\mathbf{U}_S$ and $\mathbf{U}_D$ Ekman-corrected velocities (Appendix E), where deflection angles were lower for *Sargassum*, 9° comparing to $\mathbf{U}_G$ and 4° to $\mathbf{U}_{D,d}$.

Regressing the *Sargassum* velocity against the geostrophic current $\mathbf{U}_G$ and wind gives the total effect of wind on *Sargassum* (Tab. 2), evaluated here at β_G^S=3.8% of the wind speed. This total effect includes Ekman current plus windage. Correcting *Sargassum* velocities from the Ekman currents (see Appendix E) reduces β_G^S to 2.6%, which is pure windage. Regressing the *Sargassum* velocity against the drogued drifter velocities $\mathbf{U}_{D,d}$ (15 m depth current) and wind provides a total wind effect of $\approx 3\%$ of the wind velocity, but with a better fit ($\mathbf{R^2}$=0.78 against 0.46). Removing the Ekman current, estimated windage is 2.1%.

This windage ($\approx 2\%$) is consistent with literature for undrogued SVP drifters (Brügge & Dengg, 1991; Poulain et al., 1996; Pazan & Niiler, 2001) and for *Sargassum* with a windage factor that was recently reassessed between 1-3% (Putman et al., 2020). Similarly to our results, studies on oil spill drift modelling highlighted the wind-induced drift corresponding to $\approx 2\%$ of the wind speed with a deviation angle on the right of $\approx 20 - 25°$ (Le Hénaff et al., 2012). The wind effect coefficient for *Sargassum* $\beta_D^S\%$ may not be constant. Indeed, regressions separating low and high wind cases gave values of 0.08 and 0.02 respectively (not shown). This strong dependence on wind speed may result from *Sargassum* mixing over a deeper layer as wind speed increases (Woodcock, 1993; Ody et al., 2019). The Ekman component varies very little over the first few meters, whereas windage may strongly decrease with the sinking of *Sargassum*.

Although the wind effect coefficient ($\beta_{D,d}^S$) is rather small, $\beta_{D,d}^S W$ represents on average 42% of the *Sargassum* drift velocity due to the high wind velocity. This result reinforces the view of a strong impact of wind on *Sargassum* and highlights the importance of including wind contribution into *Sargassum* drift models.

4.6. Proposed model of Sargassum drift

Drifters velocity is a good proxy for local currents (geostrophic plus Ekman). Undrogued drifters, supposedly more similar to *Sargassum* (Van Sebille et al., 2021), were associated with higher variability and lower $\mathbf{R^2}$ values than drogued drifters. Thus, the regression explaining *Sargassum* velocity with the drogued drifters and wind velocity can be exploited to better predict *Sargassum* drift. Considering the inferred parameters of Tab. 3, we propose the following *Sargassum* drift model:

$$\mathbf{U}_S = 0.8\mathbf{U} + 0.03e^{-10°i}\mathbf{W} \tag{7}$$

Where $\mathbf{U}_S$, $\mathbf{U}$ and $\mathbf{W}$ are the *Sargassum*, the total current at 15 m depth (geostrophic plus Ekman) and the wind velocities at 10 m. On average, using this model, *Sargassum* velocity of $0.36\,\mathrm{m\,s^{-1}}$ is decomposed into the contributions of current (geostrophic plus Ekman) of $0.21\,\mathrm{m\,s^{-1}}$ and wind of $0.15\,\mathrm{m\,s^{-1}}$.

Using the complex parameters proposed here allowed a gain of 4% in the $\mathbf{R^2}$ values (Tab. 3) in comparison to using real parameters ($\alpha^S_{D,d} = 1$ and $\beta^S_{D,d} = 3\%$) as in previous studies (Berline et al., 2020; Johns et al., 2020; Putman et al., 2018, 2020). However, this modest improvement corresponds on average to an error reduction of $0.13\,\mathrm{m\,s^{-1}}$, which translates into an error reduction of 1.4 km on locations over our 3 hours measurements. These results suggest that reducing the role of current to 80% of its velocity and using a wind factor of 3% deflected 10° to the right should lead to significant improvements in further drift simulations.

5. Acknowledgments

Authors thank the two reviewers that helped us to improve the manuscript clarity. We acknowledge TOSCA-CNES and IRD for funding the project SAREDA-DA allowing the production of the MODIS *Sargassum* detection dataset. AERIS-ICARE is thanked for providing processing infrastructure for the production of the dataset. The Ph.D. of Witold Podlejski is funded by ANR FORESEA (FORESEA project, grant ANR-19-SARG-0007).

Appendix A. Collocation between *Sargassum* and drifter

A collocation was defined as a situation where a drifter was close (< 20 km) from at least one detected *Sargassum* pixel (i.e. a pixel which AFAI is above the threshold defined in Wang & Hu (2016)). More specifically, the process followed those steps: 1) the Aqua and Terra timestamp (20 km median filter) was computed at every 12:00 UTC drifter position; 2) the drifter position was linearly interpolated at the average time between Aqua and Terra; 3) The scene was considered collocated if there was a *Sargassum* pixel in a box of 40 pixels around that interpolated position.

Appendix B. Matching on SIFT key points

In order to extract the *Sargassum* velocity, images were matched based on aggregates' shape. The SIFT algorithm allowed extracting key points to describe the *Sargassum* shape and position. Then, an ad-hoc algorithm was developed to search for the best 2D translation explaining the drift. The corresponding code, inspired from the RANdom SAmple Consensus (RANSAC) approach (Derpanis, 2010), is detailed in the pseudo-algorithm 1. All possible translations between the two sets of points were tested, and the one maximising the counter (thus the most likely) was retained. Images pairs with less than 4 matching points were excluded. For remaining cases, matching pairs displacements in the scene were averaged to compute one value of *Sargassum* velocity that was added to the dataset.

Algorithm 1 Translation evaluation from SIFT key points

Require: T_{pts}, A_{pts} the list of SIFT key points for Terra and Aqua images

```
for each T_pt ∈ T_pts, A_pt ∈ A_pts do
    Counter ← 0
    Translation ← A_pt − T_pt
    for each T_temp ∈ T_pts, A_temp ∈ A_pts do
        if Distance(Translation + T_temp, A_temp) ≤ 500 m then
            Counter ← Counter + 1
        end if
    end for
end for
```

Appendix C. Complex linear regression

Let $\mathbf{Z}$ be a random complex response variable with $\mathbf{X}$ and $\mathbf{Y}$ complex regressors. We have a sample $E = \{(\mathbf{X}_n, \mathbf{Y}_n, \mathbf{Z}_n), 1 \cdots N\}$ of size N of these variables. It is supposed that they are connected through a linear model of the form:

$$\mathbf{Z}_n = \alpha + \beta \mathbf{X}_n + \gamma \mathbf{Y}_n + \varepsilon_n,\ n = 1 \cdots N,$$

where α, β and γ are complex parameters that must be estimated from the sample E and ε is a (complex) remainder whose norm is hoped to be as small as possible. As usual in a regression problem, the parameter estimation is done through least squares minimization of the cost function:

$$SSE(\alpha, \beta, \gamma) = \sum_{n=1}^{N} (\mathbf{Z}_n - \alpha - \beta \mathbf{X}_n - \gamma \mathbf{Y}_n)(\mathbf{Z}_n - \alpha - \beta \mathbf{X}_n - \gamma \mathbf{Y}_n)_\star,$$

where $\mathbf{X}_\star$ denotes the complex conjugate of $\mathbf{X}$. Let construct the design matrix $M = (\mathbb{1}, X, Y)$ where $\mathbb{1}$ is the N-vector with entries $1 + i1$, $X = (\mathbf{X}_1, \ldots, \mathbf{X}_N)'$ and $Y = (\mathbf{Y}_1, \ldots, \mathbf{Y}_N)'$ the N-vectors of the complex regressors. In matrix form, the cost function writes :

$$SSE(a) = (Z - Ma)^\star (Z - Ma),$$

where $a = (\alpha, \beta, \gamma)'$ is the vector of parameters and $Z = (\mathbf{Z}_1, \ldots, \mathbf{Z}_N)'$, the vector of the response variable and $Z^\star$ its transpose conjugate. Solution of the complex regression is given when solving the normal equations for the complex regression:

$$\widehat{a} = (M^\star M)^{-1} M^\star Z$$

An estimated value of $\mathbf{Z}_n$ is then obtained with : $\widehat{\mathbf{Z}}_n = \widehat{\alpha} + \widehat{\beta} \mathbf{X}_n + \widehat{\gamma} \mathbf{Y}_n$. One can also compute the estimated errors with: $\widehat{\varepsilon}_n = \mathbf{Z}_n - \widehat{\mathbf{Z}}_n$.

Appendix D. Bootstrapped confidence intervals for parameters

Suppose now a complex regression achieved with sample E and residuals estimated with $\widehat{\varepsilon}_1, \ldots, \widehat{\varepsilon}_N$ as above. Consider a bootstrap replicate of the initial sample denoted as $E_B = \left\{(\mathbf{X}_n, \mathbf{Y}_n, \mathbf{Z}_n^B), n = 1 \cdots N\right\}$ such that $\mathbf{Z}_n^B = \widehat{\alpha} + \widehat{\beta}\mathbf{X}_n + \widehat{\gamma}\mathbf{Y}_n + \varepsilon_n^B$, where the residuals $\varepsilon_1^B, \ldots, \varepsilon_N^B$ have been drawn from an estimated distribution of the residuals that uses $\widehat{\varepsilon}_1, \ldots, \widehat{\varepsilon}_N$ as data. As these errors are complex numbers, this distribution is bivariate. It can be estimated using a Gaussian density with mean parameter being the vector of real and imaginary parts of the empirical mean error $\overline{\varepsilon} = \frac{1}{N}\sum_n \widehat{\varepsilon}_n$ and variance parameter being the empirical covariance matrix between real and imaginary parts of the $\widehat{\varepsilon}_n$.

Use now a bootstrap sample E_B to compute new estimates $\widehat{\alpha}^B$, $\widehat{\beta}^B$ and $\widehat{\gamma}^B$. As this procedure can be repeated at wish, one can estimate boundaries of a 95%-confidence intervals as the quantiles of the empirical distribution for both real and imaginary parts of $\widehat{\alpha}$, $\widehat{\beta}$ and $\widehat{\gamma}$.

Error values are simulated using bootstrapped errors obtained by sampling an estimated distribution function of the errors in place of its real unknown distribution. Bootstrapped samples of the data are then constructed and confidence intervals can be estimated for $\widehat{\alpha}$, $\widehat{\beta}$ and $\widehat{\gamma}$ considered as true coefficients of the regression instead of α, β and γ.

Appendix E. Regressions using Ekman-corrected currents

We used formulas and constants from Cushman-Roisin & Beckers (2011) for computing Ekman current. The eddy viscosity ν_E was $1 \times 10^{-2}\,\mathrm{m^2\,s^{-1}}$, the drag coefficient C_d was 1.5×10^{-3}, the air density ρ_a was $1.20\,\mathrm{kg\,m^{-3}}$ and the water density ρ_0 was $1 \times 10^3\,\mathrm{kg\,m^{-3}}$. Considering that undrogued drifters and *Sargassum* aggregates drift in the surface layer of the ocean, the Ekman current estimated at z = 0 m was removed from U_S and $U_{D,u}$. The Ekman current estimated at z = 15 m was removed from $U_{D,d}$ because of their drogue centred at 15 m depth.

Model	α	β	R^2	N_{obs}
$\mathbf{U}_S = \alpha_G^S \mathbf{U}_G + \beta_G^S \mathbf{W}$	$0.602 \pm 0.062 \exp(-8.6 \pm 7.1°i)$	0	0.11	192
	0	$0.026 \pm 0.003 \exp(-3.2 \pm 5.5°i)$	0.14	192
	$0.567 \pm 0.057 \exp(1.0 \pm 5.6°i)$	$0.026 \pm 0.002 \exp(-9.0 \pm 4.8°i)$	0.35	192
$\mathbf{U}_{D,u} = \alpha_G^{D,u} \mathbf{U}_G + \beta_G^{D,u} \mathbf{W}$	$0.757 \pm 0.081 \exp(-4.9 \pm 7.2°i)$	0	0.22	94
	0	$0.022 \pm 0.004 \exp(2.8 \pm 9.2°i)$	0.08	94
	$0.666 \pm 0.078 \exp(1.1 \pm 7.2°i)$	$0.019 \pm 0.003 \exp(-5.7 \pm 10.5°i)$	0.35	94
$\mathbf{U}_{D,d} = \alpha_G^{D,d} \mathbf{U}_G + \beta_G^{D,d} \mathbf{W}$	$0.828 \pm 0.07 \exp(5.5 \pm 4.7°i)$	0	0.42	98
	0	$0.005 \pm 0.003 \exp(32.2 \pm 108.9°i)$	-0.01∗	98
	$0.844 \pm 0.071 \exp(6.0 \pm 4.4°i)$	$0.005 \pm 0.002 \exp(-38.0 \pm 68.6°i)$	0.44	98
$\mathbf{U}_S = \alpha_{D,u}^S \mathbf{U}_{D,u} + \beta_{D,u}^S \mathbf{W}$	$0.875 \pm 0.046 \exp(-0.7 \pm 3.3°i)$	0	0.57	94
	$0.699 \pm 0.047 \exp(4.2 \pm 4.0°i)$	$0.017 \pm 0.002 \exp(-16.1 \pm 8.7°i)$	0.62	94
$\mathbf{U}_S = \alpha_{D,d}^S \mathbf{U}_{D,d} + \beta_{D,d}^S \mathbf{W}$	$0.81 \pm 0.044 \exp(-2.3 \pm 3.3°i)$	0	0.57	98
	$0.793 \pm 0.039 \exp(-1.6 \pm 2.8°i)$	$0.021 \pm 0.002 \exp(-4.0 \pm 6.0°i)$	0.74	98

Table Appendix E.1: Same as table 2 except that the velocities $\mathbf{U}_S$,$\mathbf{U}_{D,d}$ and $\mathbf{U}_{D,u}$ are corrected from Ekman current at either 0 or 15 meter depth.

References

Barton, I. J. (2002). Ocean currents from successive satellite images: The reciprocal filtering technique. *Journal of Atmospheric and Oceanic Technology*, *19*, 1677–1689.

Berline, L., Ody, A., Jouanno, J., Chevalier, C., André, J.-M., Thibaut, T., & Ménard, F. (2020). Hindcasting the 2017 dispersal of sargassum algae in the tropical north atlantic. *Marine Pollution Bulletin*, *158*, 111431.

Beron-Vera, F. J., & Miron, P. (2020). A minimal maxey–riley model for the drift of sargassum rafts. *Journal of Fluid Mechanics*, *904*.

Brooks, M. T., Coles, V. J., & Coles, W. C. (2019). Inertia influences pelagic sargassum advection and distribution. *Geophysical Research Letters*, *46*, 2610–2618.

Brooks, M. T., Coles, V. J., Hood, R. R., & Gower, J. F. (2018). Factors controlling the seasonal distribution of pelagic sargassum. *Marine Ecology Progress Series*, *599*, 1–18.

Brügge, B., & Dengg, J. (1991). Differences in drift behavior between drogued and undrogued satellite-tracked drifting buoys. *Journal of Geophysical Research: Oceans*, *96*, 7249–7263.

Chávez, V., Uribe-Martínez, A., Cuevas, E., Rodríguez-Martínez, R. E., van Tussenbroek, B. I., Francisco, V., Estévez, M., Celis, L. B., Monroy-Velázquez, L. V., Leal-Bautista, R. et al. (2020). Massive influx of

pelagic sargassum spp. on the coasts of the mexican caribbean 2014–2020: challenges and opportunities. *Water*, *12*, 2908.

Chelton, D. B., DeSzoeke, R. A., Schlax, M. G., El Naggar, K., & Siwertz, N. (1998). Geographical variability of the first baroclinic rossby radius of deformation. *Journal of Physical Oceanography*, *28*, 433–460.

Cuevas, E., Uribe-Martínez, A., & Liceaga-Correa, M. d. l. Á. (2018). A satellite remote-sensing multi-index approach to discriminate pelagic sargassum in the waters of the yucatan peninsula, mexico. *International Journal of Remote Sensing*, *39*, 3608–3627.

Cushman-Roisin, B., & Beckers, J.-M. (2011). *Introduction to geophysical fluid dynamics: physical and numerical aspects*. Academic press.

Derpanis, K. G. (2010). Overview of the ransac algorithm. *Image Rochester NY*, *4*, 2–3.

Descloitres, J., Minghelli, A., Steinmetz, F., Chevalier, C., Chami, M., & Berline, L. (2021). Revisited estimation of moderate resolution sargassum fractional coverage using decametric satellite data (s2-msi). *Remote Sensing*, *13*, 5106.

Ekman, V. W. (1905). On the influence of the earth's rotation on ocean-currents., .

Farnebäck, G. (2003). Two-frame motion estimation based on polynomial expansion. In *Scandinavian conference on Image analysis* (pp. 363–370). Springer.

Gower, J. F., & King, S. A. (2011). Distribution of floating sargassum in the gulf of mexico and the atlantic ocean mapped using meris. *International Journal of Remote Sensing*, *32*, 1917–1929.

Hersbach, H., & Dee, D. (2016). Era5 reanalysis is in production. *ECMWF newsletter*, *147*, 5–6.

Imzilen, T., Chassot, E., Barde, J., Demarcq, H., Maufroy, A., Roa-Pascuali, L., Ternon, J. F., & Lett, C. (2019). Fish aggregating devices drift like oceanographic drifters in the near-surface currents of the atlantic and indian oceans. *Progress in oceanography*, *171*, 108–127.

Johns, E. M., Lumpkin, R., Putman, N. F., Smith, R. H., Muller-Karger, F. E., Rueda-Roa, D. T., Hu, C., Wang, M., Brooks, M. T., Gramer, L. J. et al. (2020). The establishment of a pelagic sargassum population in the tropical atlantic: biological consequences of a basin-scale long distance dispersal event. *Progress in Oceanography*, *182*, 102269.

Jouanno, J., Benshila, R., Berline, L., Soulié, A., Radenac, M.-H., Morvan, G., Diaz, F., Sheinbaum, J., Chevalier, C., Thibaut, T. et al. (2021a). A nemo-based model of sargassum distribution in the tropical atlantic: description of the model and sensitivity analysis (nemo-sarg1. 0). *Geoscientific Model Development*, *14*, 4069–4086.

Jouanno, J., Moquet, J.-S., Berline, L., Radenac, M.-H., Santini, W., Changeux, T., Thibaut, T., Podlejski, W., Ménard, F., Martinez, J.-M. et al. (2021b). Evolution of the riverine nutrient export to the tropical atlantic over the last 15 years: is there a link with sargassum proliferation? *Environmental Research Letters*, *16*, 034042.

Kundu, P. K. (1976). Ekman veering observed near the ocean bottom. *Journal of Physical oceanography*, *6*, 238–242.

Kwon, K., Choi, B.-J., Kim, K. Y., & Kim, K. (2019). Tracing the trajectory of pelagic sargassum using satellite monitoring and lagrangian transport simulations in the east china sea and yellow sea. *Algae*, *34*, 315–326.

Lagerloef, G. S., Mitchum, G. T., Lukas, R. B., & Niiler, P. P. (1999). Tropical pacific near-surface currents estimated from altimeter, wind, and drifter data. *Journal of Geophysical Research: Oceans*, *104*, 23313–23326.

de Lanay, D. B., Monthieux, A., Banydeen, R., Mehdi, J.-L., Resiere, D., Drame, M., & Neviere, R. (2022). Risk of preeclampsia among women living in coastal areas impacted by sargassum strandings on the french caribbean island of martinique. *Environmental Toxicology and Pharmacology*, (p. 103894).

Le Hénaff, M., Kourafalou, V. H., Paris, C. B., Helgers, J., Aman, Z. M., Hogan, P. J., & Srinivasan, A. (2012). Surface evolution of the deepwater horizon oil spill patch: combined effects of circulation and wind-induced drift. *Environmental science & technology*, *46*, 7267–7273.

Lowe, D. G. (2004). Distinctive image features from scale-invariant keypoints. *International journal of computer vision*, *60*, 91–110.

Lucas, B. D., Kanade, T. et al. (1981). An iterative image registration technique with an application to stereo vision. Vancouver.

Lumpkin, R., & Centurioni, L. (2019). Noaa global drifter program quality-controlled 6-hour interpolated data from ocean surface drifting buoys. *NOAA: Washington, DC, USA*, .

Lumpkin, R., & Pazos, M. (2007). Measuring surface currents with surface velocity program drifters: the instrument, its data, and some recent results. *Lagrangian analysis and prediction of coastal and ocean dynamics*, *39*, 67.

Masuoka, E., Fleig, A., Wolfe, R. E., & Patt, F. (1998). Key characteristics of modis data products. *IEEE Transactions on Geoscience and Remote Sensing*, *36*, 1313–1323.

Merle, H., Resière, D., Mesnard, C., Pierre, M., Jean-Charles, A., Béral, L., & Nevière, R. (2021). Case report: Two cases of keratoconjunctivitis tied to sargassum algae emanations. *The American Journal of Tropical Medicine and Hygiene*, *104*, 403–405.

Mikolajczyk, K., & Schmid, C. (2005). A performance evaluation of local descriptors. *IEEE transactions on pattern analysis and machine intelligence*, *27*, 1615–1630.

Minghelli, A., Chevalier, C., Descloitres, J., Berline, L., Blanc, P., & Chami, M. (2021). Synergy between low earth orbit (leo)—modis and geostationary earth orbit (geo)—goes sensors for sargassum monitoring in the atlantic ocean. *Remote Sensing*, *13*, 1444.

Miron, P., Olascoaga, M., Beron-Vera, F., Putman, N., Triñanes, J., Lumpkin, R., & Goni, G. (2020). Clustering of marine-debris-and sargassum-like drifters explained by inertial particle dynamics. *Geophysical Research Letters*, *47*, e2020GL089874.

Mulet, S., Etienne, H., Ballarotta, M., Faugere, Y., Rio, M., Dibarboure, G., & Picot, N. (2021). Synergy between surface drifters and altimetry to increase the accuracy of sea level anomaly and geostrophic current maps in the gulf of mexico. *Advances in Space Research*, *68*, 420–431.

Ody, A., Thibaut, T., Berline, L., Changeux, T., André, J.-M., Chevalier, C., Blanfuné, A., Blanchot, J., Ruitton, S., Stiger-Pouvreau, V. et al. (2019). From in situ to satellite observations of pelagic sargassum distribution and aggregation in the tropical north atlantic ocean. *PLoS One*, *14*, e0222584.

Pazan, S. E., & Niiler, P. P. (2001). Recovery of near-surface velocity from undrogued drifters. *Journal of Atmospheric and Oceanic Technology*, *18*, 476–489.

Podlejski, W., Descloitres, J., Chevalier, C., Minghelli, A., Lett, C., & Berline, L. (2022). Filtering out false sargassum detections using context features. *Frontiers in Marine Science*, *9*. URL: `https://www.frontiersin.org/articles/10.3389/fmars.2022.960939`. doi:`10.3389/fmars.2022.960939`.

Poulain, P.-M., Gerin, R., Mauri, E., & Pennel, R. (2009). Wind effects on drogued and undrogued drifters in the eastern mediterranean. *Journal of Atmospheric and Oceanic Technology*, *26*, 1144–1156.

Poulain, P.-M., Warn-Varnas, A., & Niiler, P. (1996). Near-surface circulation of the nordic seas as measured by lagrangian drifters. *Journal of Geophysical Research: Oceans*, *101*, 18237–18258.

Putman, N. F., Goni, G. J., Gramer, L. J., Hu, C., Johns, E. M., Trinanes, J., & Wang, M. (2018). Simulating transport pathways of pelagic sargassum from the equatorial atlantic into the caribbean sea. *Progress in oceanography*, *165*, 205–214.

Putman, N. F., Lumpkin, R., Olascoaga, M. J., Trinanes, J., & Goni, G. J. (2020). Improving transport predictions of pelagic sargassum. *Journal of Experimental Marine Biology and Ecology*, *529*, 151398.

Resiere, D., Valentino, R., Nevière, R., Banydeen, R., Gueye, P., Florentin, J., Cabié, A., Lebrun, T., Mégarbane, B., Guerrier, G. et al. (2018). Sargassum seaweed on caribbean islands: an international public health concern. *The Lancet*, *392*, 2691.

Rodríguez-Martínez, R., Medina-Valmaseda, A., Blanchon, P., Monroy-Velázquez, L., Almazán-Becerril, A., Delgado-Pech, B., Vásquez-Yeomans, L., Francisco, V., & García-Rivas, M. (2019). Faunal mortality associated with massive beaching and decomposition of pelagic sargassum. *Marine Pollution Bulletin*, *146*, 201–205.

Sutherland, G., Soontiens, N., Davidson, F., Smith, G. C., Bernier, N., Blanken, H., Schillinger, D., Marcotte, G., Röhrs, J., Dagestad, K.-F. et al. (2020). Evaluating the leeway coefficient of ocean drifters using operational marine environmental prediction systems. *Journal of Atmospheric and Oceanic Technology*, *37*, 1943–1954.

Van Sebille, E., Aliani, S., Law, K. L., Maximenko, N., Alsina, J. M., Bagaev, A., Bergmann, M., Chapron, B., Chubarenko, I., Cózar, A. et al. (2020). The physical oceanography of the transport of floating marine debris. *Environmental Research Letters*, *15*, 023003.

Van Sebille, E., Zettler, E., Wienders, N., Amaral-Zettler, L., Elipot, S., & Lumpkin, R. (2021). Dispersion of surface drifters in the tropical atlantic. *Frontiers in Marine Science*, *7*, 607426.

Van Tussenbroek, B. I., Arana, H. A. H., Rodríguez-Martínez, R. E., Espinoza-Avalos, J., Canizales-Flores, H. M., González-Godoy, C. E., Barba-Santos, M. G., Vega-Zepeda, A., & Collado-Vides, L. (2017). Severe impacts of brown tides caused by sargassum spp. on near-shore caribbean seagrass communities. *Marine pollution bulletin*, *122*, 272–281.

Wang, M., & Hu, C. (2016). Mapping and quantifying sargassum distribution and coverage in the central west atlantic using modis observations. *Remote sensing of environment*, *183*, 350–367.

Wang, M., & Hu, C. (2020). Automatic extraction of sargassum features from sentinel-2 msi images. *IEEE Transactions on Geoscience and Remote Sensing*, *PP*, 1–19. doi:10.1109/TGRS.2020.3002929.

Wang, M., Hu, C., Barnes, B. B., Mitchum, G., Lapointe, B., & Montoya, J. P. (2019). The great atlantic sargassum belt. *Science*, *365*, 83–87.

Woodcock, A. H. (1993). Winds subsurface pelagic sargassum and langmuir circulations. *Journal of Experimental Marine Biology and Ecology*, *170*, 117–125.

Yang, H., Arnone, R., & Jolliff, J. (2015). Estimating advective near-surface currents from ocean color satellite images. *Remote Sensing of Environment*, *158*, 1–14.